A spatially resolved dataset of stable water isotopes in monthly precipitation over Jeju island, Korea (2000–2003)

Kwang-Sik Lee[1], Dong-Chan Koh[2,3], Young-Hee Kim[4], Won-Bae Park[5], Songyi Kim[4], Hyejung Jung[4], Yeon-Sik Bong[1], Woo-Jin Shin[1], Chaeyoung Kim[4], Jeonghoon Lee[4,*]

[1]Center for Earth and Planetary Material Analysis, Korea Basic Science Institute, Ochang, Chungbuk 28119, South Korea
[2]Korea Institute of Geoscience and Mineral Resources, Daejeon 34132, South Korea
[3]Geoscience, University of Science and Technology, Daejeon 34113, South Korea
[4]Dept. of Science Education (Earth Science), Ewha Womans University, Seoul 03760, South Korea
[5]The Jeju Institute, Jeju-si, Jeju-do 63147, South Korea

Correspondence to: Jeonghoon Lee (jeonghoon.d.lee@gmail.com)

Abstract. Spatially resolved, multi-year observations of stable water isotopes in precipitation remain scarce for high-relief maritime islands. We present a historical dataset of monthly precipitation isotopes collected between September 2000 and December 2003 at 15 stations on Jeju Island, South Korea, spanning elevations of 5–1,230 m a.s.l. The dataset contains 462 paired $\delta^{18}O$ and $\delta^{2}H$ measurements, deuterium excess (d-excess = $\delta^{2}H - 8 \times \delta^{18}O$), station and sampling metadata, and 488 station-month records of precipitation and air-temperature estimates, including 26 records without corresponding isotope measurements. Missing isotope observations were not imputed. Individual $\delta^{18}O$ and $\delta^{2}H$ values range from −13.2 to −2.0‰ and from −93.3 to −5.8‰, respectively, and generally exhibit lower values in summer than during the cool season. Unweighted station means for the common 2002–2003 period yield elevation gradients of −0.146 ± 0.013‰ per 100 m for $\delta^{18}O$ and −1.043 ± 0.128‰ per 100 m for $\delta^{2}H$, with uncertainties expressed as standard errors. An island–nearshore comparison with isotope-enabled model output provides context for broad seasonal variability. By recovering and openly publishing observations collected more than two decades ago, this dataset preserves a historical baseline for subsequent precipitation-isotope monitoring and hydrological studies on Jeju Island. The data are available at https://doi.org/10.22747/paper_data.20260219.42.

1 Introduction

Stable isotope compositions of precipitation ($\delta^{18}O$ and $\delta^{2}H$), together with deuterium excess ($d = \delta^{2}H - 8\times\delta^{18}O$), are widely used to investigate hydrological processes, groundwater recharge, and atmospheric water transport (Dansgaard, 1964; Lee et al., 2010; Dee et al., 2023; Jung et al., 2025). Combined with meteorological observations, such records provide an empirical basis for examining temporal variability, developing regional isoscapes, and interpreting isotope signals transferred through hydrological systems (Feng et al., 2009; Uemura et al., 2012; Konecky et al., 2020). Global monitoring networks have improved understanding of precipitation-isotope variability, but their station density is often insufficient to resolve local gradients across steep terrain. Spatially distributed observations are therefore needed to complement single-site records and

characterize seasonal variability and isotope–elevation relationships at regional and local scales (Posmentier et al., 2004; Peng et al., 2010).

In high-relief maritime settings, precipitation isotope patterns may reflect elevation, orographic uplift and progressive condensation, seasonal atmospheric circulation, and post-condensation processes (Guan et al., 2009; Lee et al., 2013; Xie et al., 2022). These processes are not unique to volcanic islands, and volcanic geology is not considered a direct control on precipitation isotope composition in this study. Jeju's volcanic setting is nevertheless hydrologically relevant because its permeable rocks promote infiltration, restrict surface runoff, and sustain groundwater-dependent water resources. Spatially resolved precipitation-isotope observations can therefore contribute to recharge studies in steep island aquifers when combined with independent hydrological evidence (Koh et al., 2012; Prada et al., 2016; Koh et al., 2022; Wang et al., 2024).

Previous studies on Jeju Island documented seasonal and elevation-related differences in precipitation isotopes but generally covered relatively short periods or limited numbers of sampling sites (Lee et al., 1999; Lee et al., 2003). Groundwater and cave studies further showed the importance of characterizing precipitation inputs, while demonstrating that interpretations of recharge and proxy records also require information on subsurface mixing, infiltration, and cave processes (Koh et al., 2012; Woo et al., 2008; Johnson and Ingram, 2004). More recently, Kim et al. (2026) combined precipitation and groundwater isotope observations with mixing analysis to investigate seasonal and elevational contributions to groundwater recharge. The present data paper complements these application-focused studies by documenting the underlying station-resolved precipitation-isotope observations and associated metadata as a reusable data product.

Here, we present $\delta^{18}O$ and $\delta^{2}H$ measurements and calculated deuterium excess values (d-excess) for 462 precipitation samples collected from September 2000 to December 2003 at 15 stations spanning 5–1,230 m a.s.l. The dataset includes associated monthly precipitation and air-temperature estimates together with station, sampling, and analytical metadata. Its multi-site design permits evaluation of seasonal variability and isotope–elevation relationships during the 39-month observation period. Because the record is time bounded, it cannot characterize interannual-to-decadal variability or independently calibrate long-term paleoclimate reconstructions. It can, however, provide an instrumental-period reference for comparison with subsequent observations and for future recharge or cave-monitoring studies when accompanied by independent process information. It also permits a broad seasonal consistency check against isotope-enabled model output, rather than direct model validation (Yoshimura et al., 2011; Konecky et al., 2020). By recovering, documenting, and openly publishing observations collected more than two decades ago, this work preserves a historical record that might otherwise remain inaccessible and extends the value of the original monitoring effort.

2 Study area and method

2.1 Geographical and climatic features of Jeju island

Jeju Island is located approximately 100 km south of the Korean Peninsula. It covers 1,845 km² and is dominated by Mt. Halla (1,950 m a.s.l.), with terrain rising from coastal plains to the central summit (Figure 1). The island consists predominantly of fractured basalt, with localized trachyte and pyroclastic deposits. The high permeability of the basalt promotes rapid infiltration and limited surface runoff, contributing to groundwater-dominated hydrology (Hahn et al., 1997; Koh et al., 2012; Kim et al., 2026). Jeju Island has a monsoon-influenced climate situated between temperate continental and subtropical maritime regimes. Regional studies describe marked seasonal contrasts in atmospheric circulation and moisture transport (Lee et al., 2013). These climatic conditions provide context for the observation period, although individual precipitation samples are not assigned to specific moisture sources or atmospheric mechanisms in the present study.

Climatically, Jeju Island lies in a transitional zone between temperate continental and subtropical maritime regimes. Its climate is strongly shaped by monsoon circulation, seasonal shifts in moisture sources, and interactions between the Siberian High and the North Pacific High. Winters (November to April) are influenced by cold, dry continental air masses, while summers (June–September) are dominated by humid maritime tropical air advected from the Pacific Ocean. During the sampling period from September 2000 to December 2003, the site-specific mean monthly air temperatures associated with the isotope-monitoring network ranged from −3.4 to 27.9 °C, with an overall mean of 12.7 °C. Annual precipitation exceeds 1,600 mm in most regions, with over half occurring during the summer monsoon period. These synoptic-scale seasonal contrasts contribute to seasonal changes in precipitation $\delta^{18}O$ and $\delta^{2}H$ values and d-excess, contributing to well-defined seasonal patterns in $\delta^{18}O$, $\delta^{2}H$, and d-excess values (Lee et al., 2013; KMA 2021). The combined influence of steep altitudinal gradients, varied moisture source trajectories, and distinct monsoon circulation patterns produces spatial and temporal variations in precipitation $\delta^{18}O$, $\delta^{2}H$, and d-excess that cannot be captured using single-station monitoring approaches. Coastal regions are predominantly influenced by marine vapor and convective rainfall, while precipitation at higher elevations is generally depleted in ^{18}O and ^{2}H relative to precipitation at lower elevations. These conditions make Jeju Island investigate altitude effects, moisture source variability, and monsoon-driven isotope seasonality using multi-site and long-term monitoring. Consequently, the spatial distribution of our 15 monitoring stations was intentionally designed to capture these gradients, extending from 10 m to over 1,500 m in elevation.

2.2 Previous stable isotopic studies on Jeju island

Previous studies on Jeju Island examined stable isotopes in precipitation, groundwater, and cave water, but the early precipitation records were generally limited in duration or spatial coverage (Lee et al., 1999; Lee et al., 2003; Woo et al., 2013). Recent work analyzed stable isotopes in monthly precipitation and groundwater together with isotope mixing to examine the seasonal and elevational origins of groundwater recharge, identifying high-elevation summer precipitation as the dominant recharge source (Kim et al., 2026). The present data paper complements that application-focused study by documenting and

openly publishing a station-resolved precipitation-isotope record and associated metadata from September 2000 to December 2003, facilitating transparent reuse and evaluation of seasonal and elevation-related patterns.

Subsequent research expanded to include the isotopic characterization of groundwater, cave dripwater, and speleothems, demonstrating that modern precipitation isotope data are essential for calibrating paleoclimate proxies in Jeju's volcanic landscapes (Woo et al., 2008; Jo et al., 2014). These studies identified that groundwater recharge is predominantly derived from high-elevation winter precipitation, while speleothem isotopic signals preserve a mixture of seasonal infiltration and moisture source variability (Lee et al., 2007; Kim et al., 2003). However, these investigations largely relied on extrapolated isotope lapse rates or interpolated GNIP data due to the absence of a spatially resolved precipitation isotope dataset collected simultaneously across multiple elevations and climatic regimes. This limitation has hindered the ability to accurately quantify spatial heterogeneity in isotopic elevation relationships, moisture source transitions, and monsoon driven fractionation processes, thereby constraining the development of reliable isoscapes and robust paleoclimate interpretations for Jeju Island (Peng et al., 2010; Ha et al., 2013).

More recent studies employed isotope-enabled models and atmospheric satellite observations to analyze moisture source trajectories and synoptic-scale vapor dynamics affecting Jeju Island (Yoshimura et al., 2011; Lee et al., 2013). These works highlighted the importance of a seasonal pattern characterized by lower precipitation $\delta^{18}O$ and $\delta^{2}H$ values in summer and higher values in winter, but validation of these model outputs was limited due to sparse in situ observations and the lack of a high-density monitoring network. The previous studies could therefore characterize either temporal changes or spatial differences, but not both concurrently. No prior study has produced a multi-year, multi-site dataset capturing both spatial and temporal variability of precipitation isotopes across volcanic terrain, which is essential for quantifying altitude effects, seasonal moisture source changes, monsoon circulation patterns, and Rayleigh distillation across elevation gradients.

Recent work on Jeju Island combined precipitation and groundwater isotope observations with mixing analysis to identify seasonal and high-elevation contributions to groundwater recharge (Kim et al., 2026). The present data paper complements that application-focused study by openly providing the complete station-resolved precipitation isotope record and associated metadata, enabling independent reuse, consistent evaluation of isotope–elevation relationships, and comparison with subsequent monitoring. The present dataset fills this critical gap by providing simultaneous spatial and temporal precipitation isotope observations from 15 stations over a continuous 39-month period. It enables, for the first time on Jeju Island, quantitative assessment of both seasonal isotope cycles and decreases in precipitation $\delta^{18}O$ and $\delta^{2}H$ values with increasing elevation, facilitating more accurate characterization of recharge dynamics, topographic gradients, and paleoenvironmental interpretations. The dataset also offers a robust observational basis for calibrating isotope-enabled climate models and for developing regional isoscape frameworks.

2.3 Sampling and analytical methods

Precipitation samples were collected continuously from September 2000 to December 2003 at 15 strategically selected stations distributed across Jeju Island (10–1,500 m a.s.l.), covering distinct topographic, climatic, and geographic features (Figure 1). The sampling network was designed to represent windward and leeward slopes, coastal-to-inland transitions, and altitudinal gradients, allowing simultaneous characterization of spatial and temporal variations in precipitation $\delta^{18}O$, $\delta^{2}H$, and d-excess. Stations were classified into four elevation zones (coastal < 100 m, lowland 100–300 m, mid-elevation 300–800 m, and high-elevation > 800 m) to quantify altitude effects and orographic precipitation processes.

In total, $\delta^{18}O$ and $\delta^{2}H$ were measured in 462 precipitation samples, and d-excess was calculated as $d = \delta^{2}H - 8 \times \delta^{18}O$. Analyses were conducted using an Isoprime isotope ratio mass spectrometer (IRMS) at the Korea Basic Science Institute (KBSI), following IAEA protocols. $\delta^{18}O$ measurements were performed using CO_2–H_2O equilibration and cryogenic condensation, whereas $\delta^{2}H$ was analyzed by chromium reduction (Cr-Pyrolysis) to generate H_2 gas. Analytical precision was ± 1.0‰ for $\delta^{2}H$ and ± 0.1‰ for $\delta^{18}O$, based on repeated internal standards calibrated against VSMOW2, SLAP2, and GISP reference waters. All reported values follow the conventional δ-notation relative to VSMOW:

$$\delta = \left(\frac{R_x}{R_{\mathrm{VSMOW}}} - 1\right) \times 1000 \quad (1)$$

where R_x is the ratio of heavy to light isotopes ($^{18}O/^{16}O$ or $^{2}H/H$) in the sample.

During compilation of the released dataset, we did not apply a statistical outlier threshold to $\delta^{18}O$, $\delta^{2}H$, or d-excess. We retained the single exclusion reported by Lee et al. (2002). A May 2001 sample identified as ST-3 in that study had $\delta^{18}O$ = −1.9‰ and $\delta^{2}H$ = −33‰, with a d-excess value of −17.8‰. Lee et al. (2002) reported that the sample departed strongly from the meteoric-water-line relationship, interpreted this as evidence of substantial evaporation before analysis, and excluded it from their calculations. We therefore also excluded this sample from the released observations and from all analyses reported here. Its identifier, values, cross-reference, and exclusion rationale are retained in the Excluded_Samples worksheet for traceability. No additional archived measurement was removed during the present compilation solely because its $\delta^{18}O$, $\delta^{2}H$, or d-excess value was relatively high or low. The released dataset contains the remaining 462 paired $\delta^{18}O$ and $\delta^{2}H$ measurements. Site–month combinations without a valid archived isotope measurement remain missing and were neither reconstructed nor imputed. Precipitation and air-temperature records were not used as numerical isotope-screening criteria.

3 Results and discussion

3.1 Temporal variations of precipitation isotopes

Precipitation $\delta^{18}O$ and $\delta^{2}H$ values and d-excess ($d = \delta^{2}H - 8\times\delta^{18}O$) varied seasonally during the 39-month observation period from September 2000 to December 2003 (Figure 2). Monthly mean $\delta^{18}O$ and $\delta^{2}H$ values were generally lower during summer, particularly from June to September, and relatively higher during winter from November to February although the timing and magnitude varied among years. The seasonal minima in $\delta^{18}O$ and $\delta^{2}H$ broadly coincided with the main summer-monsoon precipitation period, whereas the seasonal maxima occurred during the relatively dry winter period. Across the 462 individual samples, $\delta^{18}O$ ranged from −13.2‰ to −2.0‰, $\delta^{2}H$ from −93.3‰ to −5.8‰, and d-excess from 3.3‰ to 29.1‰. The individual station-level $\delta^{18}O$ observations are shown in Fig. S1, and island-wide monthly means are shown with the corresponding meteorological series in Figure 2. This pattern indicates that precipitation during the peak summer monsoon carries the most isotopically depleted signatures, reflecting intensified convective activity, long-distance moisture transport, and enhanced Rayleigh distillation associated with summer precipitation. In contrast, isotopic enrichment during winter precipitation is likely related to lower atmospheric humidity, stronger sub-cloud evaporation, and increased contributions from drier continental air masses during the cold season (Tao et al., 2025).

Unlike $\delta^{18}O$ and $\delta^{2}H$, the secondary isotope parameter d-excess shows a more complex seasonal evolution, characterized by a quadratic rather than sinusoidal pattern, indicating a stronger sensitivity to kinetic fractionation processes (Dansgaard, 1964). Monthly d-excess values are lowest during summer months, consistent with highly humid maritime moisture sources, whereas significantly higher winter d-excess values are consistent with seasonal changes in source-region humidity and evaporation conditions; however, no unique moisture-source attribution is made from d-excess alone. These seasonal behaviors were further supported by correlation analysis, which showed that d-excess exhibited the strongest inverse relationship with air temperature ($R^2 = 0.77$, $p < 0.0001$) compared to $\delta^{18}O$ ($R^2 = 0.07$) and $\delta^{2}H$ ($R^2 = 0.29$), confirming its higher sensitivity to moisture source humidity and evaporation conditions (Table 1). The broad seasonal cycle is consistent with changes in East Asian monsoon circulation, precipitation amount, transport history, and condensation along air-mass pathways (Lee et al., 2003, 2013). The present monthly dataset does not provide event-scale trajectories or process diagnostics, however, so individual samples are not assigned to specific moisture sources and the observed variations are not attributed to a single mechanism (Guo et al., 2021).

Seasonal analysis of the local meteoric water lines (LMWLs) further reveals systematic variations in $\delta^{18}O$ vs $\delta^{2}H$ relationships associated with changes in atmospheric circulation and moisture source conditions over Jeju Island (Figure 3; Table 2). The annual LMWL derived from the full dataset ($\delta^{2}H = 8.17 \times \delta^{18}O + 15.72$, $R^2 = 0.89$) reflects the integrated influence of both summer monsoon and winter precipitation regimes, but seasonal regressions demonstrate clear contrasts between warm and cold seasons (Fritz et al., 2022). During the summer monsoon period (JJAS), the LMWL exhibits a relatively higher slope and a markedly lower intercept, consistent with precipitation dominated by humid maritime moisture sources and extensive rainout under convective conditions, which suppresses kinetic fractionation during evaporation. In

contrast, the winter LMWL (NDJF) is characterized by a reduced slope and an elevated intercept, indicating enhanced kinetic effects associated with lower humidity, stronger evaporation at the moisture source, and increased contributions from continental air masses transported over the Yellow Sea. Transitional seasons display intermediate LMWL characteristics, reflecting the gradual shift between these two dominant circulation regimes. These seasonal differences in LMWL geometry are consistent with the observed seasonal behavior of d-excess and corroborate the interpretation that moisture source humidity and atmospheric transport pathways exert a first-order control on isotope relationships in precipitation. The well-resolved seasonal LMWLs presented here provide a robust reference framework for interpreting groundwater recharge processes, cave dripwater isotopes, and paleoclimate archives in monsoon-influenced volcanic island environments, where mixing of seasonal signals can otherwise obscure the climatic interpretation of isotope records.

Recurring annual variability in monthly $\delta^{18}O$ and $\delta^{2}H$ was summarized empirically as $\delta(t) = C + A \sin[2\pi(t - \varphi)/12]$, where t is calendar month, C is the fitted baseline, A is amplitude, and φ is phase (Figure 4). Unlike conventional raw isotopic time-series, the seasonal cycle parameters (baseline, amplitude, and phase) extracted from the periodic fitting approach allow direct input into hydrological and land-surface models that require temporally smoothed isotope forcing data (Nelson et al., 2021). This is particularly valuable in monsoon climates, where conventional amount-weighted averages do not capture seasonal variability in moisture source or atmospheric circulation. The documented seasonal cycle also defines a reference framework for distinguishing between temperature-based fractionation (winter isotopic enrichment) and moisture-source depletion (summer monsoon rainout)**,** facilitating attribution of isotope variation to underlying atmospheric processes rather than simple temperature effects. The secondary isotopic parameter, d-excess, however, exhibited a more complex seasonal pattern, deviating from pure sinusoidal behavior. Its strong inverse relationship with temperature and relative humidity confirms that d-excess can serve as an effective indicator of moisture source humidity, ocean–atmosphere evaporation conditions, and sub-cloud kinetic fractionation during transport (Schoenemann et al., 2016). This sensitivity makes d-excess particularly valuable for identifying shifts between continental (high d-excess) and maritime (low d-excess) moisture sources, especially during winter and summer seasons, respectively. When integrated with satellite water vapor isotope datasets (e.g., TES, TROPOMI) or isotope-enabled reanalysis, the dataset can help improve representations of monsoon moisture recycling, boundary layer humidity, and airmass trajectory modeling (Worden et al., 2007). The fitted $\delta^{18}O$ and $\delta^{2}H$ baselines are −6.97‰ and −41.13‰, with amplitudes of 1.22‰ and 13.90‰, respectively. The corresponding R^2 values (0.26 and 0.42) show that the sine functions capture only part of the observed interannual and station-level variability. They are therefore descriptive summaries, not mechanistic representations of isotope processes or monthly climatological normals. d-excess was summarized with a quadratic calendar-month curve because its observed seasonal distribution was not symmetric. d-excess may be influenced by source-region humidity and evaporation, cloud processes, and sub-cloud exchange, among other factors. Low or high d-excess values are consequently not assigned here to a binary maritime-versus-continental source interpretation.

3.2 Spatial variations and isotope–elevation relationships

The spatial distribution of precipitation isotopes across Jeju Island demonstrates strong topographic control, primarily driven by orographic uplift, Rayleigh distillation, and varying exposure to maritime air masses. As shown in Figure 5, $\delta^{18}O$ and $\delta^{2}H$ values exhibit progressive depletion with increasing elevation, forming a distinct altitudinal gradient characteristic of mountainous volcanic terrains. Based on 462 precipitation samples across 15 stations, $\delta^{18}O$ decreased at an average rate of −1.5‰ per 1000 m, with a strong linear fit ($R^2 = 0.88$, $p < 0.005$), while $\delta^{2}H$ showed a corresponding trend of −11‰ per 1000 m ($R^2 = 0.77$). These lapse rates are broadly consistent with those reported for other high-relief island environments in East Asia and the western Pacific, consistent with progressive rainout during orographic uplift.

While $\delta^{18}O$ and $\delta^{2}H$ showed clear elevation-driven depletion trends, d-excess displayed weaker spatial dependence, with only modest changes across elevation groups ($R^2 = 0.39$). Higher d-excess values at mid- and high-altitude locations indicate potential influence of drier continental air masses and moisture recycling during winter months, while lower values in coastal stations reflect more humid maritime moisture and stronger kinetic fractionation at the ocean–atmosphere interface. The combined analysis of $\delta^{18}O$, $\delta^{2}H$, and d-excess suggests that spatial variability in precipitation isotopes on Jeju Island is shaped not only by orographic lifting but also by seasonal shifts in moisture sources and varying humidity conditions during condensation and transport. The spatially resolved dataset presented here is the first to quantify the simultaneous effects of altitude, topographic orientation, and monsoon circulation on precipitation isotopes across Jeju Island. These results provide a robust observational basis for estimating groundwater recharge elevations, refining local isoscape models, and improving isotope-enabled hydrological simulations in volcanic island settings. Furthermore, the observed spatial gradients serve as critical calibration inputs for interpreting isotopic signals preserved in speleothems, cave dripwater, and other paleoclimate archives, contributing to improved proxy-based climate reconstructions in East Asia.

To examine spatial heterogeneity, the monitoring stations were grouped into northern, southern, eastern, and western sectors (Figure 6). To avoid confounding the comparisons with unequal station record lengths, station means were calculated over the common 2002–2003 network period. Across all 15 stations spanning 5–1,230 m a.s.l., precipitation $\delta^{18}O$ and $\delta^{2}H$ values decreased significantly with elevation at rates of −0.146 ± 0.013‰ and −1.043 ± 0.128‰ per 100 m, respectively ($\delta^{18}O$: $R^2 = 0.913$, $p < 0.001$; $\delta^{2}H$: $R^2 = 0.837$, $p < 0.001$; Table 3). The sector-specific $\delta^{18}O$ gradients ranged from −0.105 to −0.155‰ per 100 m, while the corresponding $\delta^{2}H$ gradients ranged from −0.682 to −1.158‰ per 100 m. However, each sector comprised only three or four stations and covered a different elevation range. These sector-specific regressions should therefore be regarded as exploratory, and the separate fits do not demonstrate that the slopes differ significantly among sectors. Moreover, because sample-resolved wind and atmospheric-trajectory information is unavailable, the observed sector patterns cannot be attributed uniquely to marine influence, prevailing wind direction, topographic shielding, or windward–leeward position. The network-wide regressions provide the most robust first-order description of elevation-related variation in precipitation $\delta^{18}O$ and $\delta^{2}H$ during the common observation period (Wang et al., 2024).

Examining altitudinal gradients along multiple cardinal directions provides further clarity on the spatial complexity of isotope fractionation across Jeju. This multidirectional perspective disentangles purely altitude-driven depletions from other spatial influences, such as the proximity to marine air masses or the prevailing wind trajectories. By constructing isotopic transects from north, south, east, and west, it becomes possible to pinpoint anisotropic depletion patterns and better discern localized controls on isotopic variability. These data, in turn, enhance the spatial resolution of isotope-based models and strengthen our capacity to predict recharge elevations and groundwater flow paths. The ability to distinguish between low-elevation recharge derived from coastal precipitation and high-elevation recharge sourced from more depleted rainfall is especially valuable for managing volcanic island aquifers, which often exhibit complex stratigraphy and vulnerability to contamination. Ultimately, integrating cardinal-direction transects with altitude effect analyses offers a comprehensive approach to understanding both the spatial and altitudinal dimensions of precipitation isotope variability, supporting improved water resource management and more nuanced paleoclimate reconstructions.

Previous satellite, IsoGSM, and 120 h HYSPLIT backward-trajectory analyses demonstrated seasonally contrasting atmospheric transport pathways over Jeju Island (Lee et al., 2013). These results provide regional atmospheric context for the possible influence of circulation on the directional lapse rates. However, because event-specific wind and trajectory information is not available for each monthly precipitation sample, the differences among the directional lapse rates cannot be attributed uniquely to particular airflow regimes. They are therefore interpreted as being consistent with combined differences in slope exposure, orographic ascent, and seasonal circulation rather than as direct evidence of a specific circulation mechanism.

Although precipitation isotope composition is affected by multiple atmospheric and meteorological processes, the observed isotope–elevation relationships provide a first-order empirical basis for developing a regional precipitation isoscape. The network-wide lapse rates can be used to estimate expected modern precipitation $\delta^{18}O$ and $\delta^{2}H$ values at elevations where direct observations are unavailable. The directional analyses additionally indicate whether separate relationships may be required for different slope sectors, although such subdivision should be applied only where supported by the regression results and station coverage. A regional precipitation isoscape would be particularly useful for cave and speleothem studies on Jeju Island because precipitation isotope composition is rarely measured directly at individual cave sites. Applying the observed isotope–elevation relationships to the elevation and geographical setting of a cave can provide an initial estimate of the modern precipitation isotope input to its recharge system. This estimate can help define the plausible precipitation end-member from which soil water, epikarst water, and cave dripwater are derived.

The estimated precipitation input does not directly calibrate a speleothem record because the transfer of an isotope signal from precipitation to speleothem calcite is additionally influenced by seasonal recharge weighting, evaporation, soil and epikarst storage, cave hydrology, water–rock interaction, and calcite precipitation processes. Nevertheless, the isoscape provides an important initial constraint for evaluating this transfer when direct precipitation isotope measurements at the cave elevation are unavailable.

3.3 Comparison with IsoGSM4 output and potential relevance to paleoclimate interpretation

The 39-month dataset across Jeju Island provides one of the few datasets in East Asia that captures both the amplitude and phase of seasonal isotopic cycles, allowing for robust quantification of seasonal offsets in $\delta^{18}O$, $\delta^{2}H$, and d-excess. Unlike short-duration event-based sampling campaigns or single-site monitoring records, this dataset enables assessment of multi-year seasonal stability, which is essential for calibrating isotope-enabled climate models, such as IsoGSM and iCESM, and for validating isotopic proxies preserved in groundwater and speleothem archives (Yoshimura et al., 2011; Brady et al., 2019). The consistent occurrence of isotopic minima during summer (June to September) and maxima during winter (November to February) supports its application in seasonal weighting of recharge, particularly in volcanic aquifers where infiltration timing determines groundwater residence and isotope signatures.

To evaluate how well an isotope-enabled general circulation model reproduces the observed seasonal isotope variability over Jeju Island, we compared the observations with output from IsoGSM4 (IsoGSM-HR), the latest version of the isotope-incorporated Global Spectral Model, which simulates the fractionation and transport of stable water isotopes within a global atmospheric general circulation model (Yoshimura et al., 2008; Bong and Yoshimura, 2025). The simulation was run at T248 spectral resolution, corresponding to a horizontal grid spacing of approximately 50 km, and was nudged to the ERA5 reanalysis so that the simulated synoptic-scale circulation follows the observed atmospheric evolution; this allows a direct, month-by-month comparison between the simulated and observed precipitation isotope compositions over the observation period (September 2000 to December 2003). Monthly mean precipitation $\delta^{18}O$ and $\delta^{2}H$ values were obtained from the published model output (Bong and Yoshimura, 2025a, 2025b; https://doi.org/10.5281/zenodo.14681370 and https://doi.org/10.5281/zenodo.15073235). At this resolution, Jeju Island is covered by three model grid cells, centered at 33.31° N and 126.09° E, 126.56° E, and 127.03° E, corresponding to the western, central, and eastern parts of the island, respectively. Monthly values with simulated precipitation below 0.2 mm/day were excluded, because the isotopic composition of near-zero precipitation amounts is numerically unstable and not physically meaningful. For each month, the mean and standard deviation of $\delta^{18}O$, $\delta^{2}H$, and d-excess across the three grid cells were computed, and the ±1 standard deviation range was used to construct the shaded band shown in Figure 7, which is compared with the monthly mean observations averaged over all fifteen stations.

The mean model-minus-observation differences during May–October were +0.3‰ for $\delta^{18}O$, +1.2‰ for $\delta^{2}H$, and −1.2‰ for d-excess, whereas the corresponding differences during November–April were +1.4‰, +5.9‰, and −5.1‰, respectively (Figure 7). The differences were therefore smaller during May–October than during November–April. However, the approximately 50 km grid cannot resolve Jeju Island's detailed topography, station-scale isotope–elevation relationships, or local-to-mesoscale precipitation processes. The comparison does not determine whether the seasonal differences arise from unresolved topography, land–sea contrasts, spatial representativeness, or parameterized cloud and precipitation processes. Resolving these contributions would require additional process diagnostics and an isotope-enabled convection-permitting

regional model or an appropriately configured non-hydrostatic framework such as NICAM-WISO (Tanoue et al., 2023). The IsoGSM4 comparison is therefore used only to assess broad seasonal consistency and is not considered a validation of the observations or a process-attribution analysis.

During summer, particularly during the early-summer Changma season, precipitation over Jeju Island is strongly influenced by the Changma front, the Korean sector of the Meiyu–Baiu frontal system, and its associated large-scale moisture transport. Southwesterly flow along the western to northwestern flank of the western North Pacific subtropical high transports warm, moist air toward the Korean Peninsula, promoting moisture convergence and precipitation over Jeju Island and adjacent regions (Ninomiya and Akiyama, 1992; Lee et al., 2003; Kim et al., 2010).

When combined with independent cave-hydrological information, the dataset may also help assess how precipitation-isotope variability is transferred into cave dripwater. For example, comparisons between the precipitation record and contemporaneous or subsequent dripwater measurements may assist in evaluating whether a cave system integrates precipitation approximately across the year or preferentially reflects recharge during particular seasons. The observed range of precipitation $\delta^{18}O$ values can provide an initial reference against which the magnitude and variability of dripwater $\delta^{18}O$ are evaluated. Similarly, the elevation dependence of precipitation $\delta^{18}O$ may help constrain the range of possible recharge elevations. These comparisons could support the development and testing of conceptual or numerical models describing the transfer of precipitation through soil, epikarst, and cave systems. They cannot, however, determine recharge seasonality or elevation without independent hydrological evidence.

The temporal coverage of the dataset imposes an additional limitation. The record extends for 39 months from September 2000 to December 2003 and can characterize spatial patterns and recurring seasonal variability during that interval. It is too short to quantify interannual-to-decadal variability, establish a long-term precipitation-isotope climatology, or determine whether the observed seasonal and elevation-related relationships remained stationary outside the monitoring period. The monthly samples may also integrate multiple precipitation events and atmospheric pathways, preventing event-specific moisture sources or transport histories from being identified. Moreover, the dataset does not include contemporaneous observations of cave dripwater, cave temperature, infiltration, or speleothem calcite. It therefore cannot provide a stand-alone calibration or validation of paleoclimate reconstructions.

4 Data availability

The station-resolved precipitation isotope observations, calculated d-excess, meteorological records, metadata, and screening documentation are available in the released workbook through the Geo Big Data Open Platform at https://doi.org/10.22747/paper_data.20260219.42 (Lee et al., 2026). The IsoGSM4 (IsoGSM-HR) model output used for the

model–observation comparison is openly available at https://doi.org/10.5281/zenodo.14681370 and https://doi.org/10.5281/zenodo.15073235 (Bong and Yoshimura, 2025a, 2025b).

5 Summary

This study presents a spatially resolved dataset of stable water isotopes in precipitation collected across Jeju Island, South Korea. The dataset comprises 462 paired $\delta^{18}O$ and $\delta^{2}H$ measurements from 15 stations spanning elevations from 5 to 1,230 m a.s.l. during a 39-month monitoring period between September 2000 and December 2003. It also includes calculated d-excess values, meteorological observations, and station, sampling, analytical, and screening metadata. No statistical isotope-outlier threshold was applied; one previously documented sample affected by post-collection evaporation was excluded, and missing isotope observations were not imputed. The observations document both temporal and spatial variability in precipitation isotopes within a coordinated island-wide network. Monthly $\delta^{18}O$ and $\delta^{2}H$ values were generally lower during summer and higher during parts of the cool season. For station means over the common 2002–2003 network period, $\delta^{18}O$ and $\delta^{2}H$ decreased with elevation by -0.146 ± 0.013‰ and -1.043 ± 0.128‰ per 100 m, respectively, whereas d-excess increased by 0.126 ± 0.040‰ per 100 m. Sector-specific regressions are considered exploratory because each sector contains only three or four stations with different elevation ranges. The principal value of this dataset lies in its simultaneous coverage of seasonal variability and isotope–elevation relationships across Jeju Island's steep topographic gradient. Its recovery and open publication preserve historical observations that might otherwise remain inaccessible and provide a documented baseline for comparison with subsequent precipitation-isotope monitoring on Jeju Island. The IsoGSM4 comparison is retained only as a limited island-scale check on broad seasonal consistency. Although the 39-month record cannot characterize long-term climate variability or independently calibrate paleoclimate reconstructions, its spatial coverage, supporting metadata, and transparent documentation make it a useful resource for independent hydrological and isotope studies.

Author contributions. This study was conceptualized by KL and DK. Data were collected and analyzed by WP, YB, SK, HJ, CK and WS. The paper was written by YK and JL, with contributions from all authors.

Competing interests. The contact author has declared that none of the authors has any competing interests.

Acknowledgements. The authors thank Kei Yoshimura and Hayoung Bong for sharing their model data.

Financial support. This work was financially supported by a National Research Foundation of Korea (NRF2022R1A2C3007047) and partially supported by a grant (C638100) from the Korea Basic Science Institute. Additional support was partially provided by the Korea Environment Industry & Technology Institute through Aquatic Ecosystem Conservation Research Program, funded by the Korean Ministry of Environment (RS-2024-00332851) and the Basic Research

Project (25-3411) of the Korea Institute of Geoscience and Mineral Resources (KIGAM), funded by the Ministry of Science and ICT.

References

Brady, E., Stevenson, S., Bailey, D., Liu, Z., Noone, D., Nusbaumer, J., Otto-Bliesner, B. L., Tabor, C., Tomas, R., Wong, T., Zhang, J., and Zhu, J.: The Connected Isotopic Water Cycle in the Community Earth System Model Version 1, Journal of Advances in Modeling Earth Systems, 11, 2547–2566, https://doi.org/10.1029/2019ms001663, 2019.

Craig, H.: Isotopic variations in meteoric waters, Science, 133, 1702–1703, https://doi.org/10.1126/science.133.3465.1702, 1961.

Dansgaard, W.: Stable isotopes in precipitation, Tellus, 16, 436–468, https://doi.org/10.1111/j.2153-3490.1964.tb00181.x, 1964.

Dee, S., Bailey, A., Conroy, J. L., Atwood, A., Stevenson, S., Nusbaumer, J., and Noone, D.: Water isotopes, climate variability, and the hydrological cycle: recent advances and new frontiers, Environmental Research: Climate, 2, https://doi.org/10.1088/2752-5295/accbe1, 2023.

Feng, X., Faiia, A. M., and Posmentier, E. S.: Seasonality of isotopes in precipitation: A global perspective, Journal of Geophysical Research: Atmospheres, 114, https://doi.org/10.1029/2008jd011279, 2009.

Fritz, M., Wetterich, S., McAlister, J., and Meyer, H.: A new local meteoric water line for Inuvik (NT, Canada), Earth System Science Data, 14, 57–63, https://doi.org/10.5194/essd-14-57-2022, 2022.

Guan, H., Simmons, C. T., and Love, A. J.: Orographic controls on rain water isotope distribution in the Mount Lofty Ranges of South Australia, Journal of Hydrology, 374, 255–264, https://doi.org/10.1016/j.jhydrol.2009.06.018, 2009.

Guo, X., Gong, X., Shi, J., Guo, J., Domínguez-Villar, D., Lin, Y., Wang, H., and Yuan, D.: Temporal variations and evaporation control effect of the stable isotope composition of precipitation in the subtropical monsoon climate region, Southwest China, Journal of Hydrology, 599, https://doi.org/10.1016/j.jhydrol.2021.126278, 2021.

Ha, K., Yoon, Y. Y., Lee, K. Y., Cho, S. Y., and Ko, K. S.: Seasonal variation in the isotopic contents of precipitation in Korea, Journal of Radioanalytical and Nuclear Chemistry, 296, 389–395, https://doi.org/10.1007/s10967-012-2077-3, 2012.

Hahn, J., Lee, Y., Kim, N., Hahn, C., and Lee, S.: The groundwater resources and sustainable yield of Cheju volcanic island, Korea, Environmental Geology, 33, 43–53, 1997. https://doi.org/10.1007/s002540050223

Hassanzadeh, A., Valdivielso, S., Vazquez-Sune, E., Criollo, R., and Corbella, M.: An open source Python library for environmental isotopic modelling, Sci Rep, 13, 1895, https://doi.org/10.1038/s41598-023-29073-2, 2023.

Jo, K. N., Woo, K. S., Yi, S., Yang, D. Y., Lim, H. S., Wang, Y., Cheng, H., and Edwards, R. L.: Mid-latitude interhemispheric hydrologic seesaw over the past 550,000 years, Nature, 508, 378–382, https://doi.org/10.1038/nature13076, 2014.

Johnson, K. R. and Ingram, B. L.: Spatial and temporal variability in the stable isotope systematics of modern precipitation in China: implications for paleoclimate reconstructions, Earth and Planetary Science Letters, 220, 365–377, https://doi.org/10.1016/s0012-821x(04)00036-6, 2004.

Jung, H., Ahn, J., Iwahana, G., and Lee, J.: Understanding water flowpaths and origins in an Arctic Alaskan basin: Implications for permafrost hydrology under global warming, Advances in Climate Change Research, 16, 361–372, https://doi.org/10.1016/j.accre.2025.03.001, 2025.

Kim, M.-C., Shin, W.-J., Koh, E.-H., Koh, C.-S., Kim, G.-E., and Lee, K.-S.: Stable isotope signatures of precipitation and implications for groundwater recharge on Jeju volcanic island, South Korea, Journal of Hydrology: Regional Studies, 64, https://doi.org/10.1016/j.ejrh.2026.103141, 2026.

Kim, Y., Lee, K. S., Koh, D. C., Lee, D. H., Lee, S. G., Park, W. B., Koh, G. W., and Woo, N. C.: Hydrogeochemical and isotopic evidence of groundwater salinization in a coastal aquifer: a case study in Jeju volcanic island, Korea, Journal of Hydrology, 270, 282–294, https://doi.org/10.1016/S0022-1694(02)00307-4, 2003.

Koh, D.-C., Ha, K., Lee, K.-S., Yoon, Y.-Y., and Ko, K.-S.: Flow paths and mixing properties of groundwater using hydrogeochemistry and environmental tracers in the southwestern area of Jeju volcanic island, Journal of Hydrology, 432-433, 61–74, https://doi.org/10.1016/j.jhydrol.2012.02.030, 2012.

Koh, E. H., Lee, E., Lee, K. K., and Moon, D. C.: Integrated application of a Bayesian mixing model, numerical model, and environmental tracers to characterize groundwater recharge sources in a mountainous area, Sci Total Environ, 853, 158619, https://doi.org/10.1016/j.scitotenv.2022.158619, 2022.

Konecky, B. L., McKay, N. P., Churakova, O. V., Comas-Bru, L., Dassié, E. P., DeLong, K. L., Falster, G. M., Fischer, M. J., Jones, M. D., Jonkers, L., Kaufman, D. S., Leduc, G., Managave, S. R., Martrat, B., Opel, T., Orsi, A. J., Partin, J. W., Sayani, H. R., Thomas, E. K., Thompson, D. M., Tyler, J. J., Abram, N. J., Atwood, A. R., Cartapanis, O., Conroy, J. L., Curran, M. A., Dee, S. G., Deininger, M., Divine, D. V., Kern, Z., Porter, T. J., Stevenson, S. L., and von Gunten, L.: The Iso2k database: a global compilation of paleo-δ18O and δ2H records to aid understanding of Common Era climate, Earth System Science Data, 12, 2261–2288, https://doi.org/10.5194/essd-12-2261-2020, 2020.

Lee, J., Feng, X., Faiia, A. M., Posmentier, E. S., Kirchner, J. W., Osterhuber, R., and Taylor, S.: Isotopic evolution of a seasonal snowcover and its melt by isotopic exchange between liquid water and ice, Chemical Geology, 270, 126–134, https://doi.org/10.1016/j.chemgeo.2009.11.011, 2010.

Lee, J., Worden, J., Koh, D.-C., Yoshimura, K., and Lee, J.-E.: A seasonality of δD of water vapor (850-500 hPa) observed from space over Jeju Island, Korea, Geosciences Journal, 17, 87–95, https://doi.org/10.1007/s12303-013-0003-5, 2013.

Lee, K. S., Grundstein, A. J., Wenner, D. B., Choi, M. S., Woo, N. C., and Lee, D. H.: Climatic controls on the stable isotopic composition of precipitation in Northeast Asia, Climate Research, 23, 137–148, 2003. https://doi.org/10.3354/cr023137

Lee, K.-S., Kim, J.-M., Lee, D.-R., Kim, Y., and Lee, D.: Analysis of water movement through an unsaturated soil zone in Jeju Island, Korea using stable oxygen and hydrogen isotopes, Journal of Hydrology, 345, 199–211, https://doi.org/10.1016/j.jhydrol.2007.08.006, 2007.

Lee, K., Ko, D., Kim, H., Park, Y., Kim, S., Jeong, H., Moon, W., Shin, J., Kim, H., and Lee, J.: *Water stable isotope data of precipitation in Jeju Island*, Geo Big Data Open Platform, https://doi.org/10.22747/paper_data.20260219.42, 2026.

Lee, S., Shimada, J., and Kayane, I.: Stable isotopes in precipitation in the volcanic island of Cheju, Korea, Hydrological Processes, 13, 113–121, https://doi.org/10.1002/(sici)1099-1085(199901)13:1<113::Aid-hyp698>3.0.Co;2-p, 1999.

Nelson, D. B., Basler, D., and Kahmen, A.: Precipitation isotope time series predictions from machine learning applied in Europe, Proc Natl Acad Sci U S A, 118, https://doi.org/10.1073/pnas.2024107118, 2021.

Peng, T.-R., Wang, C.-H., Huang, C.-C., Fei, L.-Y., Chen, C.-T. A., and Hwong, J.-L.: Stable isotopic characteristic of Taiwan's precipitation: A case study of western Pacific monsoon region, Earth and Planetary Science Letters, 289, 357–366, https://doi.org/10.1016/j.epsl.2009.11.024, 2010.

Posmentier, E. S., Feng, X., and Zhao, M.: Seasonal variations of precipitation δ18O in eastern Asia, Journal of Geophysical Research: Atmospheres, 109, https://doi.org/10.1029/2004jd004510, 2004.

Prada, S., Cruz, J. V., and Figueira, C.: Using stable isotopes to characterize groundwater recharge sources in the volcanic island of Madeira, Portugal, Journal of Hydrology, 536, 409–425, https://doi.org/10.1016/j.jhydrol.2016.03.009, 2016.

Schoenemann, S. W. and Steig, E. J.: Seasonal and spatial variations of 17Oexcess and dexcess in Antarctic precipitation: Insights from an intermediate complexity isotope model, Journal of Geophysical Research: Atmospheres, 121, https://doi.org/10.1002/2016jd025117, 2016.

Tao, S., Xu, J., Xia, J., and Xiao, Y.: Influence of Sub-Cloud Evaporation on Precipitation Isotopes: Insights From Hourly-Scale Meteorological Assessment in a Large Lake in the East Asian Monsoon Region, Hydrological Processes, 39, https://doi.org/10.1002/hyp.70152, 2025.

Uemura, R., Masson-Delmotte, V., Jouzel, J., Landais, A., Motoyama, H., and Stenni, B.: Ranges of moisture-source temperature estimated from Antarctic ice cores stable isotope records over glacial–interglacial cycles, Climate of the Past, 8, 1109–1125, https://doi.org/10.5194/cp-8-1109-2012, 2012.

Wang, S., Wang, L., Yang, G., Xiao, Y., Argiriou, A. A., Shi, Y., Lei, S., and Zhang, M.: Altitude effect of precipitation isotopes in an arid mountain-basin system: Observation and modelling around the world's second-largest shifting desert, Journal of Hydrology, 636, https://doi.org/10.1016/j.jhydrol.2024.131351, 2024.

Wang, S., Wang, S., Huang, X., Wang, H., Han, Y., Wang, S., and Qi, S.: Groundwater composition and stable isotopes as proxies to investigate paleoclimate change in permafrost thawing regions, Applied Geochemistry, 169, https://doi.org/10.1016/j.apgeochem.2024.106036, 2024.

Woo, K. S., Jo, K. N., Yi, S. H., Yang, D. Y., and Li, H.-C.: Paleoclimatic investigation using oxygen isotope compositions of the YC-1 stalagmite, Yeongcheon Cave, Jeju Island, Korea for the past 600 years, Journal of the Geological Society of Korea, 49, 339–350, 2013.

Woo, K. S., Kim, J. C., Choi, D. W., Kim, J. K., Kim, R., and Nehza, O.: The origin of erratic calcite speleothems in the Dangcheomul Cave (lava tube cave), Jeju Island, Korea, Quaternary International, 176-177, 70–81, https://doi.org/10.1016/j.quaint.2007.05.009, 2008. https://doi.org/10.1016/j.quaint.2007.05.009

Worden, J., Noone, D., Bowman, K., Tropospheric Emission Spectrometer Science, T., and Data, c.: Importance of rain evaporation and continental convection in the tropical water cycle, Nature, 445, 528–532, https://doi.org/10.1038/nature05508, 2007.

Xie, C., Zhao, L., Eastoe, C. J., Liu, X., Wang, N., Zhang, Z., Dong, X., and Liu, H.: Precipitation stable isotope composition, moisture sources, and controlling factors in Xi'an, Northwest China, Atmospheric Research, 280, https://doi.org/10.1016/j.atmosres.2022.106428, 2022.

Yoshimura, K., Frankenberg, C., Lee, J., Kanamitsu, M., Worden, J., and Röckmann, T.: Comparison of an isotopic atmospheric general circulation model with new quasi-global satellite measurements of water vapor isotopologues, Journal of Geophysical Research, 116, https://doi.org/10.1029/2011jd016035, 2011.

Table 1. Correlations between isotopic compositions of precipitation and meteorological parameters

	Air temperature			Precipitation amount		
	Slope	R^2	p	Slope	R^2	p
$\delta^{18}O$	–0.07	0.07	0.10	–0.0021	0.024	0.34
$\delta^{2}H$	–1.34	0.29	0.0003	–0.047	0.15	0.014
d-excess	–0.76	0.77	0.0001	–0.031	0.52	0.0001

475 *R^2 and p denote the coefficient of determination and p-value, respectively*

Table 2. Summary of previous studies defining the local meteoric water line (LMWL)

	Sampling duration	Locality in Jeju island	Relationships
S. Lee et al. (1999)	12 months	12 locations	All: $\delta^2H = 8.39 \times \delta^{18}O + 18.59$ (n^a=12)
Lee et al. (2003)	24 months	Seongsan	All: $\delta^2H = (8.38 \pm 0.33) \times \delta^{18}O + (19.15 \pm 0.85)$ (R^2=0.85, n=109) S (JJAS, R^2=0.98, n=43) $\delta^2H = (7.94 \pm 0.20) \times \delta^{18}O + (8.87 \pm 1.46)$ W (NDJF, R^2=0.98, n=43): $\delta^2H = (6.88 \pm 0.52) \times \delta^{18}O + (20.79 \pm 3.17)$
Lee et al. (2007)	12 months	a small research site	S (JJA, R^2=0.999, n=3) $\delta^2H = 8.434 \times \delta^{18}O + 11.06$ W (NDJ, R^2=0.999, n=3): $\delta^2H = 8.70 \times \delta^{18}O + 27.22$
Ha et al. (2013)	12 months	9 locations	S (JJA, R^2=0.99, n=27) $\delta^2H = 7.73 \times \delta^{18}O + 4.82$ W (DJF, R^2=0.83, n=19): $\delta^2H = 6.05 \times \delta^{18}O + 13.58$
Our study	39 months	15 locations	All: $\delta^2H = (8.17 \pm 0.13) \times \delta^{18}O + (15.72 \pm 0.97)$ (R^2=0.89, n=462, p^b<0.0001) S (JJAS, R^2=0.96, n=156) $\delta^2H = (7.91 \pm 0.13) \times \delta^{18}O + (8.02 \pm 1.10)$ W (NDJF, R^2=0.98, n=148): $\delta^2H = (7.68 \pm 0.12) \times \delta^{18}O + (19.59 \pm 0.91)$

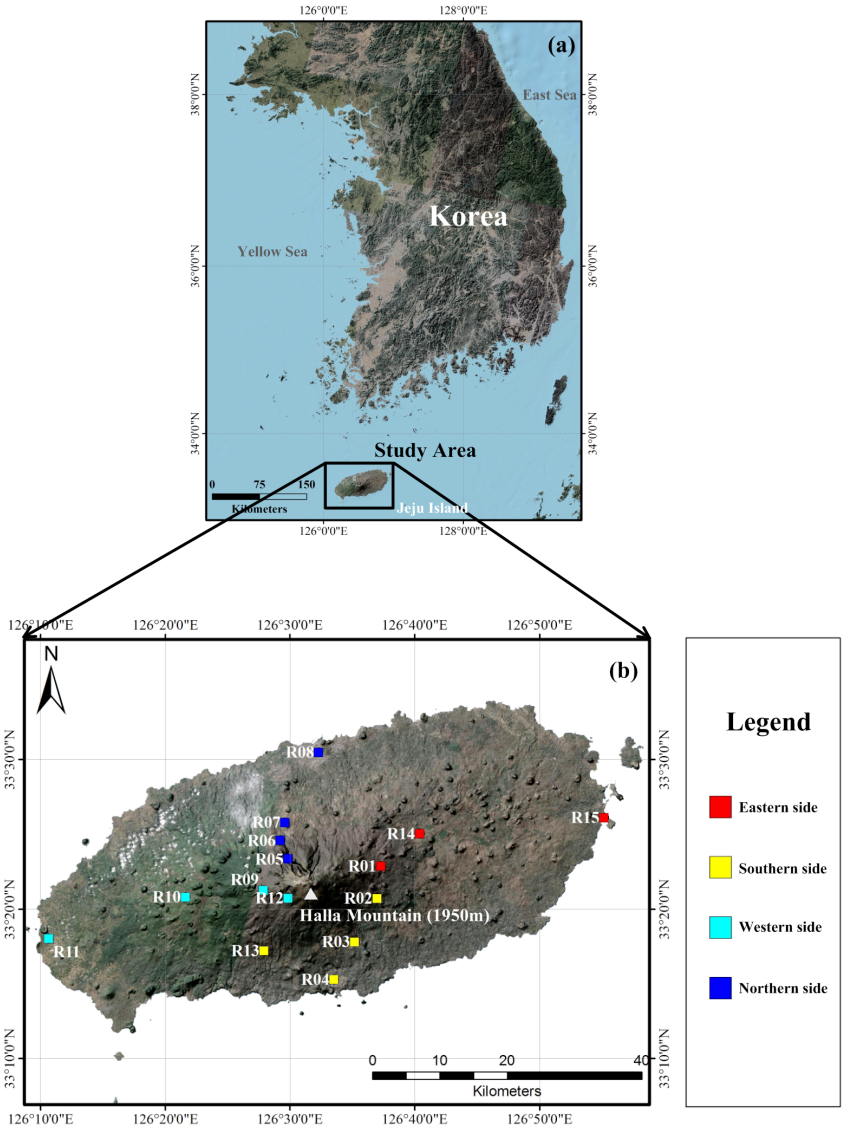
a: number of samples

b: probability

Table 3. Linear regression equations of precipitation isotopes and altitude for each cardinal direction

	Cardinal direction	Gradient (per 100 m)	R^2	p
$\delta^{18}O$	All (15; 5–1230 m)	–0.146 ± 0.013	0.913	< 0.001
	North (4; 60–960 m)	–0.155 ± 0.019	0.972	0.014
	South (4; 90–600 m)	–0.105 ± 0.030	0.862	0.071
	East (3; 5–750 m)	–0.129 ± 0.029	0.953	0.139
	West (4; 20–1230 m)	–0.141 ± 0.015	0.978	0.011
$\delta^{2}H$	All (15; 5–1230 m)	–1.043 ± 0.128	0.837	< 0.001
	North (4; 60–960 m)	–1.158 ± 0.146	0.969	0.016
	South (4; 90–600 m)	–0.682 ± 0.251	0.787	0.113
	East (3; 5–750 m)	–0.793 ± 0.019	0.999	0.015
	West (4; 20–1230 m)	–0.984 ± 0.142	0.960	0.020
d-excess	All (15; 5–1230 m)	0.126 ± 0.040	0.429	0.008
	North (4; 60–960 m)	0.081 ± 0.004	0.996	0.002
	South (4; 90–600 m)	0.154 ± 0.032	0.920	0.041
	East (3; 5–750 m)	0.241 ± 0.211	0.566	0.458
	West (4; 20–1230 m)	0.147 ± 0.027	0.938	0.032

485



490 **Figure 1. Locations of the 15 precipitation sampling stations on Jeju Island, South Korea. (a) Regional setting of Jeju Island relative to the Korean Peninsula. (b) Distribution of the monitoring stations, grouped into northern, southern, eastern, and western sectors and spanning elevations of 5–1,230 m a.s.l. The location of Mt. Halla is also indicated.**

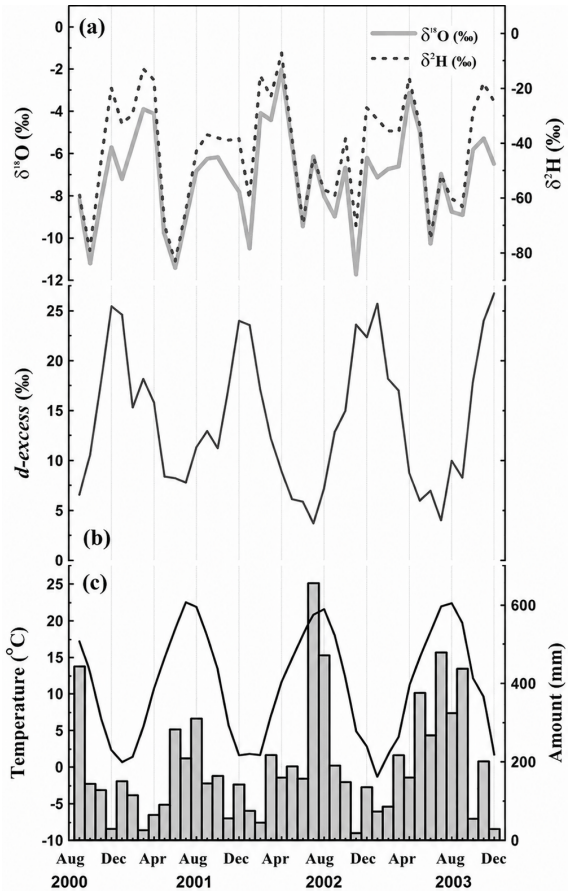


Figure 2. Monthly variations in precipitation isotopes and associated meteorological conditions on Jeju Island, South Korea, from September 2000 to December 2003. (a) Precipitation $\delta^{18}O$ and $\delta^{2}H$, (b) d-excess, and (c) mean air temperature (line) and precipitation amount (bars). Monthly values represent unweighted averages across stations with available data for each variable and observation month. Meteorological values are archived site-specific estimates derived from nearby Korea Meteorological Administration stations. The number of contributing stations varies among months and variables; missing observations were not imputed.

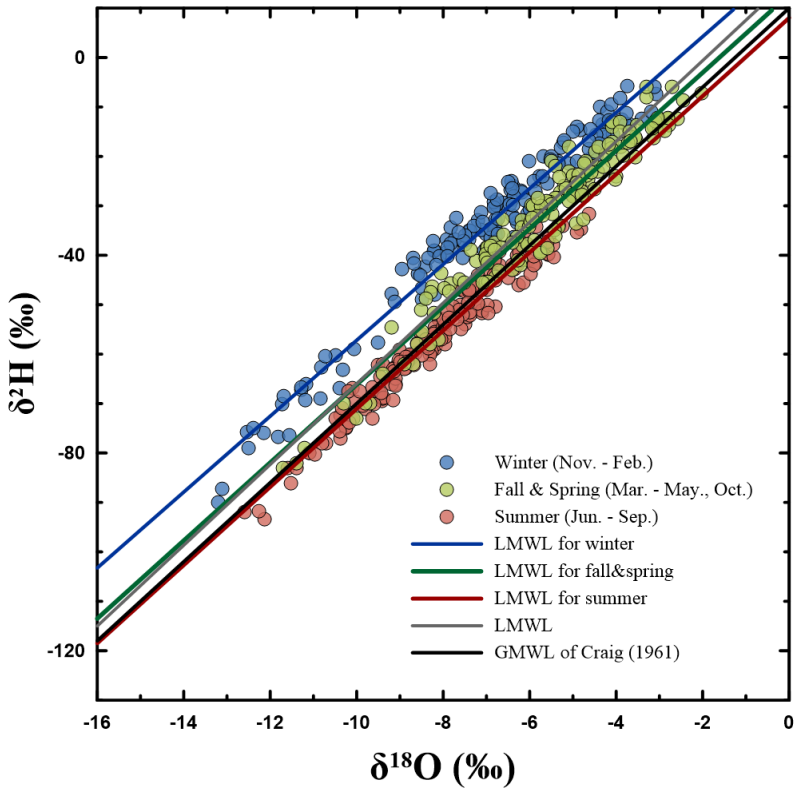


Figure 3. Local meteoric water lines (LMWLs) for precipitation on Jeju Island, South Korea. Individual samples are grouped by observation month into summer (June–September; JJAS), winter (November–February; NDJF), and transitional months (March–May and October). Seasonal regression lines summarize the observed $\delta^{18}O$–$\delta^{2}H$ relationships, with the global meteoric water line (GMWL; Craig, 1961) shown for reference.

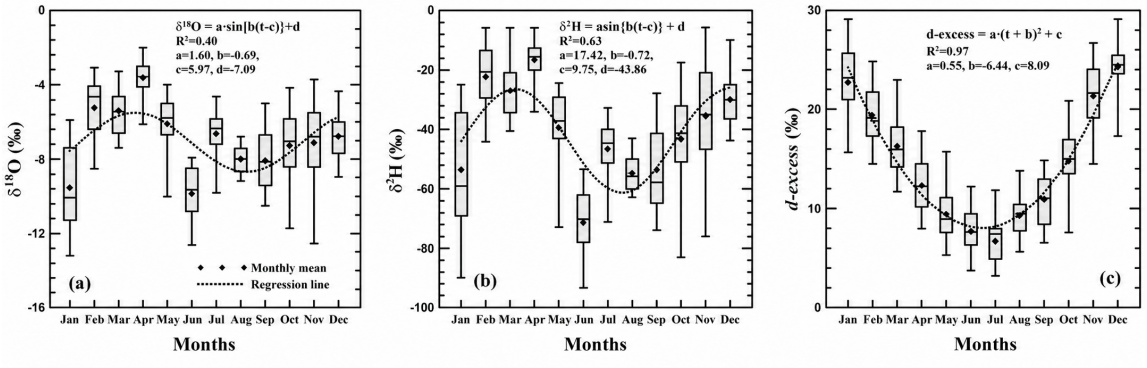


Figure 4. Calendar-month variations in precipitation isotopes on Jeju Island, South Korea. Seasonal patterns in (a) $\delta^{18}O$ and (b) $\delta^{2}H$ are summarized using sinusoidal functions with a fixed 12-month period, while (c) d-excess is summarized using a quadratic function. The fitted curves provide empirical descriptions of seasonal variability during the observation period. Boxes span the 25th–75th percentiles, and whiskers indicate the minimum and maximum values.

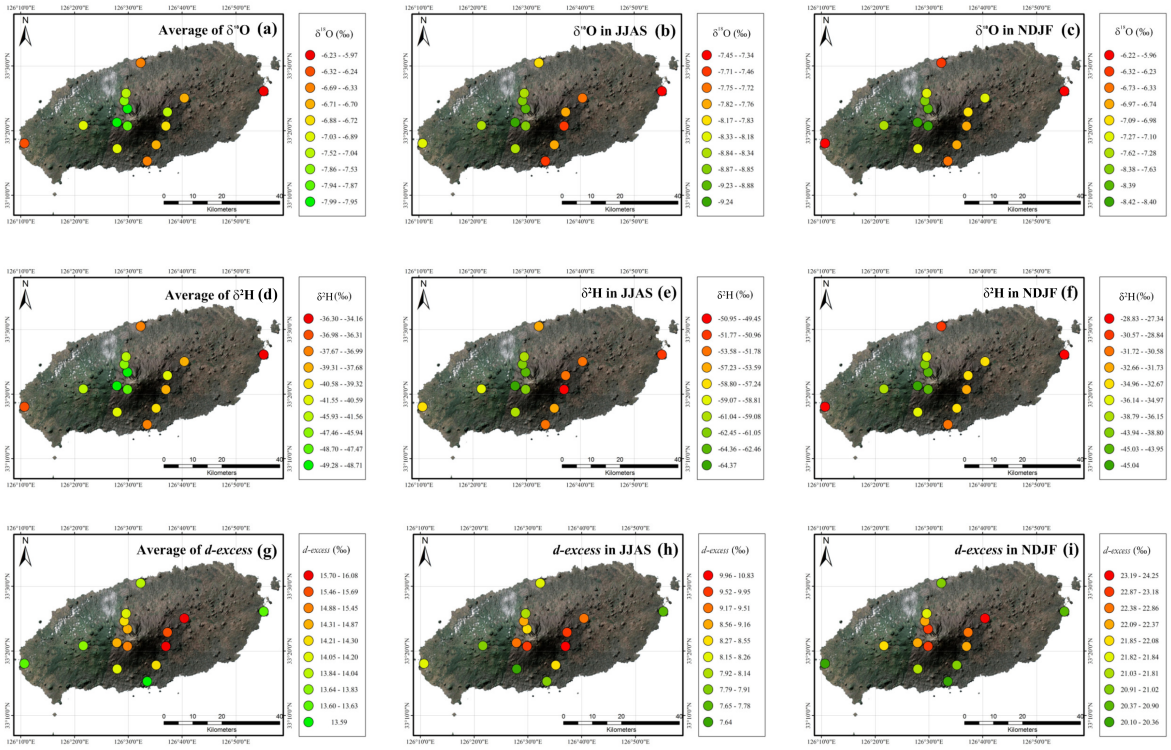


Figure 5. Spatial distributions of station-mean precipitation δ¹⁸O (a–c), δ²H (d–f), and d-excess (g–i) on Jeju Island, South Korea. Columns show overall means (a, d, g), summer means (June–September; JJAS; b, e, h), and winter means (November–February; NDJF; c, f, i), calculated from available observations at each station. Symbols indicate monitoring locations, and colors represent the corresponding station-mean isotope values.

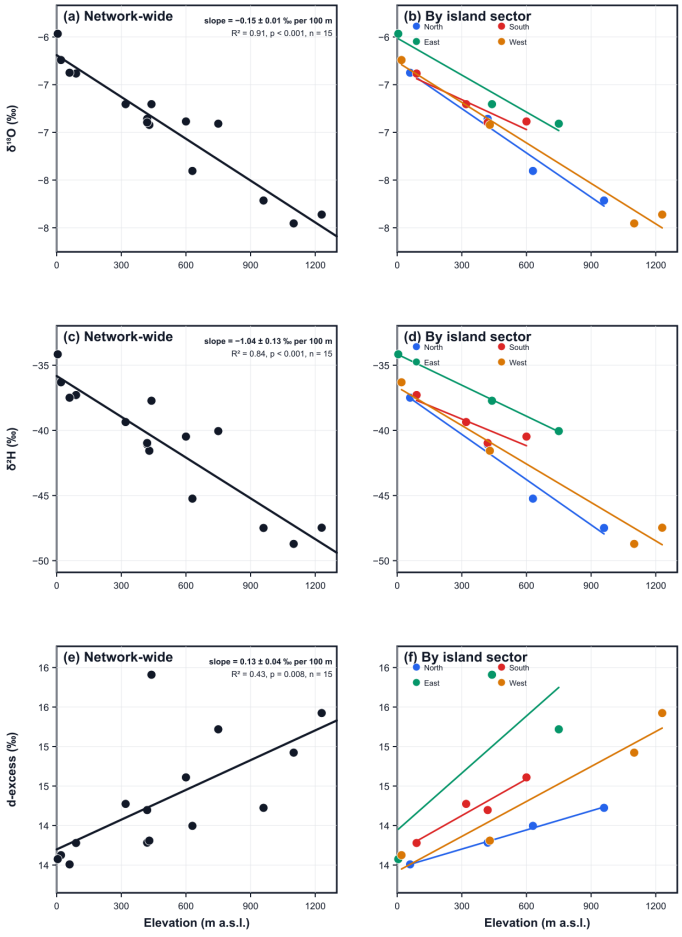


Figure 6. Relationships between station elevation and precipitation $\delta^{18}O$ (a, b), $\delta^{2}H$ (c, d), and d-excess (e, f) on Jeju Island, South Korea. Values represent unweighted station means calculated from available observations over the common 2002–2003 period. Panels (a), (c), and (e) show all 15 station means and the network-wide linear regressions. Panels (b), (d), and (f) show separate regressions for the northern, southern, eastern, and western sectors. Reported gradient uncertainties are standard errors. Sector-specific regressions are exploratory because each sector contains only three or four stations; separate fits do not establish statistically significant differences among sector slopes.

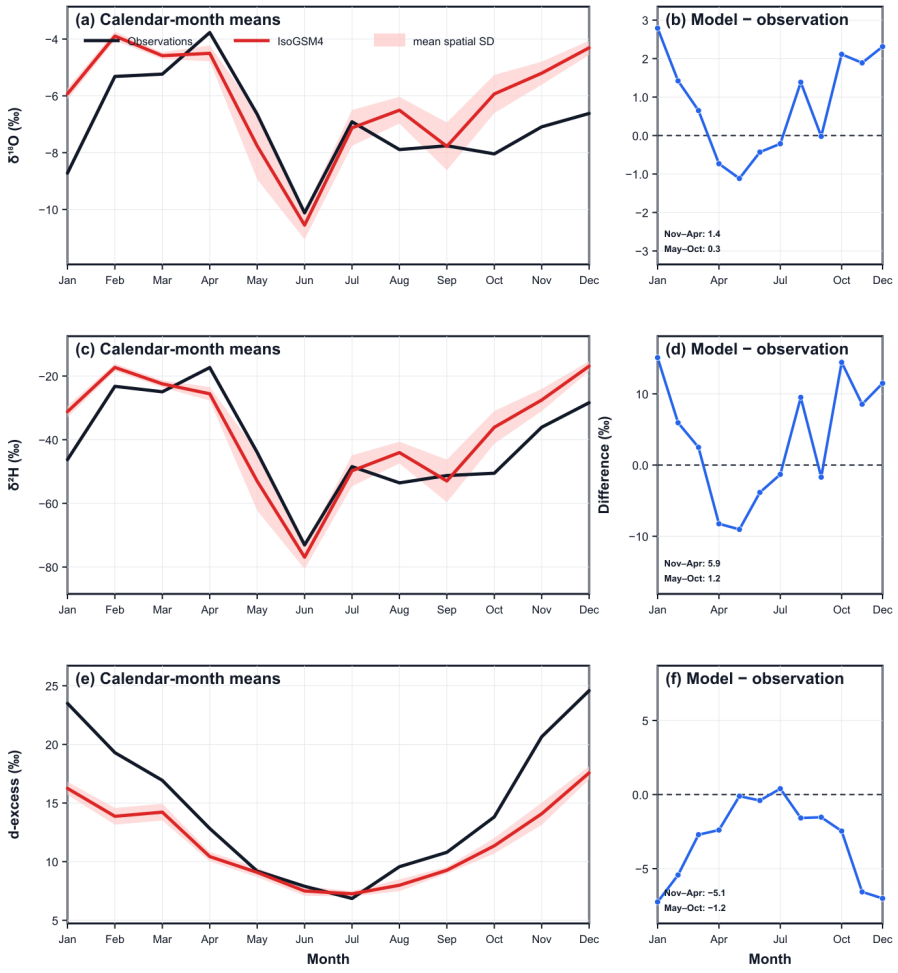


Figure 7. Calendar-month comparison of precipitation-isotope observations and IsoGSM4 output for $\delta^{18}O$ (a, b), $\delta^{2}H$ (c, d), and d-excess (e, f). Left panels show calendar-month means derived from unweighted monthly averages of available station observations (black) and retained values from three neighboring IsoGSM4 grid points (red). Red shading denotes ±1 standard deviation across the retained model grid points, representing spatial variability rather than model uncertainty. Right panels show IsoGSM4-minus-observation differences for each calendar month. Comparisons use matched observation months between September 2000 and December 2003. Model grid-point values with monthly mean precipitation below 0.2 mm d^{-1} were excluded before spatial averaging. The central grid point is located on Jeju Island, while the western and eastern points are offshore; their mean therefore represents an island–nearshore regional approximation.